Real-time, time–frequency mapping of event-related cortical activation

Real-time, time–frequency mapping of event-related cortical activation

Connie Cheung[1,2,3] **and Edward F Chang**[1,2,3,4]

[1] Department of Neurological Surgery, UC San Francisco, CA, USA
[2] Graduate Program in Bioengineering, UC Berkeley-UC San Francisco, CA, USA
[3] Center for Integrative Neuroscience, UC San Francisco, CA, USA

E-mail: connie_cheung@berkeley.edu and ChangEd@neurosurg.ucsf.edu

Abstract
Functional mapping of eloquent cortex is a common and necessary component of neurosurgical operative planning. Current electrical stimulation-based techniques are inefficient, can evoke seizures and are prone to false-negative results. Here, we present a novel cortical mapping system that extracts event-related neural activity from passive electrocorticographic recordings to quickly and accurately localize sensory and motor cortices using the precise temporal properties of spectral alteration. This procedure generates a robust functional motor and sensory cortical map in seconds, and usually with less than five to ten trial events. Our algorithm demonstrates high concordance with results derived using independent electrical cortical stimulation mapping.

S Online supplementary data available from stacks.iop.org/JNE/9/046018/mmedia

(Some figures may appear in colour only in the online journal)

Introduction

Cortical mapping is a critical tool in safely carrying out neurosurgical procedures near 'eloquent' brain regions. The traditional method for brain mapping is electrical cortical stimulation (ECS) [1–4]. Since only one site can be tested at a given time and must often be tested repetitively for confirmation, it is a highly inefficient method and can misrepresent important information about distributed cortical operations [5–7]. Cortical stimulation evokes unwanted seizures in up to 50% of cases [7–9]. Furthermore, ECS mapping can be highly operator dependent, and despite comprehensive ECS mapping, patients can have neurologic impairments [3, 4, 10, 11].

An alternative to ECS is measuring evoked cortical activity while patients are engaged in normal physiologic behavior. Electrocorticography (ECoG), which refers to direct recordings via electrodes placed on the cerebral cortex, can provide an accurate representation of spatiotemporal neural activity when sampling from a broad cortical surface

[12–17]. Recent studies have revealed that high gamma frequencies (>60Hz) are an extremely discrete spatial and temporal marker of neural activity [12, 13, 18]. Previous investigations have been largely constrained to offline analyses with a few exceptions of online application [19–23]. In particular, several groups have demonstrated impressive passive localization of functional cortex [20–23]. However, these recent demonstrations involve algorithms that effectively average signal across time, thus discarding temporal information that could be instrumental to understanding important dynamics, such as latency differences between activation in sensory, motor and cognitive processes. If temporal information were to be retained, such dynamical differences could provide clinicians with important insight into differing cortical functionality (e.g. motor versus somatosensory). This information can affect surgical planning decisions that drastically minimize morbidity [3, 4, 8, 10, 11]. For example, patients can usually tolerate parasthesias from sensory cortex resection, but paralysis from inadvertent motor cortex injury is extremely debilitating. Furthermore, cognitive processes are often redundant or more distributed, and those

---

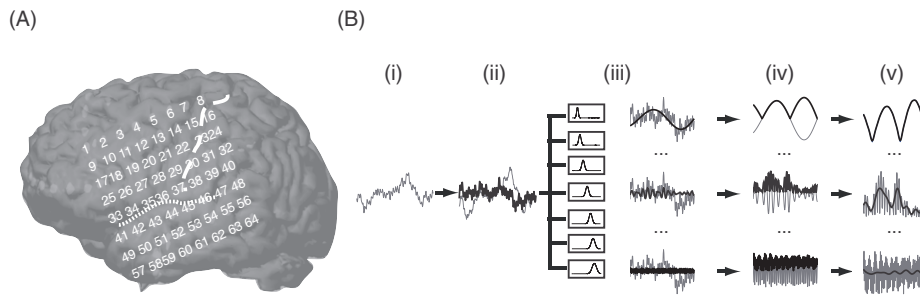[4] Author to whom any correspondence should be addressed.

Figure 1. ECoG grid superimposed on patient brain and real-time signal-processing algorithm. (A) A 64-channel subdural ECoG electrode array implanted over subject A's left lateral hemisphere. Electrode numbers are superimposed on the 3D MR surface reconstruction image. The central sulcus and Sylvian fissure are outlined with dashed and dotted lines, respectively. (B) The real-time signal-processing algorithm is depicted. (i) An example of the raw ECoG signal from a single channel. (ii) Line noise is eliminated and the signal is re-referenced to the common average signal. (iii) The signal is separated by a filter bank (4–7, 8–12, 13–30, 31–59, 61–110, 111–179, 181–260 Hz). (iv) The absolute value of the time series is taken. (v) The approximate amplitude envelope of the signal is extracted by low-pass filtering (cutoff frequencies: 5, 5, 20, 20, 40, 40, 40 Hz). The resulting signal after the stepwise process has been performed is shown in black. The preceding signal before the processing step is shown in gray.

Table 1. Patient characteristics.

Subject	Age	Gender	Hemispheric coverage	Epilepsy type	Age of seizure onset	Resection location	Engel seizure outcome classification	Hemispheric dominance for language (Wada)	Major cognitive deficits
A	23	Male	Left	Focal	3	Temporal lobe	I	Left	No
B	36	Female	Left	Focal	18	Inferior parietal lobe	II	Left	No
C	48	Male	Left	Focal	2	Anterior temporal lobe	I	Left	No
D	45	Male	Left	Focal	24	Posterior temporal cortex	I	Left	No
E	30	Male	Right	Focal	7	Inferior parietal cortex	III	Left	No

impairments are more likely to recover from injury compared to deficits in basic sensorimotor processing [24–26].

Our goal was to develop a robust, reliable and accurate system capable of performing real-time brain mapping based upon spectral changes evoked by brain activity during physiologic behavioral conditions. Intuitive visualization allows for rapid identification of spatial and temporal patterns during functional cortical activation with potential to supplement or replace ECS.

Materials and methods

Subjects

We recorded ECoG in five refractory epilepsy patients (see table 1) undergoing intracranial monitoring for the localization of an epileptogenic focus. Subjects underwent a craniotomy for chronic (1–2 weeks) implantation of a subdural platinum–iridium electrode array over either the left or right hemisphere. The study protocol, approved by the UC San Francisco Committee on Human Research, presented minimal risk to participating subjects and did not interfere with the clinical recordings. Placement of the array was determined entirely by clinical needs and varied between subjects. All participants provided informed consent.

For the purpose of this paper, the majority of the subject-specific figures were generated from a representative example (subject A). Using proprietary anatomic image fusion software from BrainLab (Munich, Germany), electrode positions were extracted by computed tomography (CT) scan, co-registered with the patient's MRI and then superimposed on the

subject's 3D MRI surface reconstruction image (figure 1(A)). Registrations were verified with intraoperative photographs, and by another third-party open-source imaging software, Osirix.

Experimental setup

For the majority of the subjects (A–D), the subdural ECoG grids implanted were standard 64-channel platinum–iridium electrodes with 10 mm center-to-center spacing arranged in an 8 × 8 configuration (Ad-Tech, Racine, WI, USA). Each electrode had an exposed diameter of 2 mm. Subject E received a high-density 256-channel grid with 4 mm center-to-center spacing over the right hemisphere. Each electrode had exposed diameter of 1.25 mm.

ECoG signals were split between the clinical monitoring system and a customized research data acquisition and processing system. The ground and reference signals were split from a scalp electrode, usually on the patient's forehead. A 30 s baseline rest period dataset was collected. During this baseline period, the room was quieted and subjects were instructed to simply rest with eyes open without moving. Generally, only one baseline collection was needed per day of experimentation; however, multiple were often collected for posthoc comparisons, or if there was a long interval between data collection periods.

Experimental sessions were divided into blocks, each lasting 1–2 min. There were four simple tasks designed to illustrate the algorithm: (1) speaking, (2) listening, (3) hand button press and (4) tactile hand somatosensation. Each block consisted of 15–40 repeated trials of the same task.

The speaking task involved self-paced production of /ba/ and /la/ syllables. The listening task involved simple passive listening to the experimenter's repeated production of speech syllables. The third task required the subject to press a handheld button press device with the thumb of the contralateral hand. Subjects were instructed to press the button when a cue was presented. In the fourth task, to isolate the somatosensory response, the experimenter briefly applied the same button press device against the subject's finger while the subject was resting.

Real-time spectral mapping

To rapidly identify spatial and temporal patterns in ECoG signal during functional cortical activation, the following algorithm was implemented.

Signal acquisition. First, ECoG signal was acquired in real-time using a portable customized multichannel neurophysiology workstation (Tucker-Davis Technologies, TDT, Alachua, FL, USA). All channel signals were amplified independently. The data were sampled at 500 Hz and recorded in a circular buffer for real-time analysis.

Real-time signal processing. Real-time signal processing was carried out on the portable workstation. To ensure that signals analyzed contained no ambient electrical line noise, 60 Hz and its harmonics were removed using a second-order Butterworth notch filter with a 5 Hz stopband. The common average reference was then removed from each channel by subtracting the average of the raw signal across all electrodes. Electrode channels were omitted if they, upon visual inspection, had poor signal quality due to electrode drift, poor electrode contact or excessive high-frequency noise. Following the re-referencing, the signal was band pass filtered at seven different frequency bands (4–7, 8–12, 13–30, 31–59, 61–110, 111–179, 181–260 Hz) using a second-order Butterworth filter. The resulting bandpass signals can be viewed as carrier signals whose amplitudes are modulated by slower periodic signals.

The slower periodic signal can be extracted by approximating the envelope of the bandpass signal. This was done by low-pass filtering the absolute value of the resulting signal. Since the cutoff frequency of a modulating signal is always at most half the bandwidth of the bandpass signal, frequency cutoffs were set at 5, 20 and 40 Hz for signals band passed filtered between 4–12, 13–59 and 61–260 Hz, respectively. A schematic diagram of the preprocessing stream can be seen in figure 1(B).

Event detection. A basic event detection method was implemented in order to determine the timing of cortical events related to the execution of a particular task. Both speaking and listening events were recorded using a microphone. For the hand movement and somatosensory tasks, a simple button press device was used. Both analog signals were recorded synchronously with the multichannel ECoG data. The signal was converted to a digital signal and downsampled to 500 Hz

and smoothed using an exponential smoothing average with a factor of 0.005. Threshold voltages were predetermined for the outputs of the microphone at 80 dB sound pressure level (SPL) and the button press device. Event onset was defined to be the time when analog voltage exceeded the predefined threshold voltage. To ensure that inaccuracy in event detection did not skew any results, any experimental session was discarded where false events (e.g. coughing) were registered.

Visualization. To allow for rapid visual identification of spatial and temporal patterns, MATLAB (Mathworks, Natick, MA, USA) was used for visualization. The envelopes of the ECoG signal and event signal were used as inputs to our customized program.

To examine the event-related change in ECoG activity, the neural signal was normalized with respect to the baseline rest signal. The log power of the signal was first calculated by taking the logarithm of the incoming envelope signal. To avoid taking the logarithm of 0, which is undefined, the median envelope signals during the baseline period were added as constants prior to taking the logarithm. The log power was then z-score normalized using the mean and standard deviation of the baseline log power signal.

During the task, five plots of the entire electrode grid were continuously refreshed. This means that the software was set to read and analyze newly acquired data immediately after the previous cycle was completed. Each cycle took on average 0.7 s to complete, with each plot taking approximately 0.10–0.15 s to calculate and display. Listed below are names and descriptions of the plots.

(1) *Average plot*: It displays the running average event-related spectrogram. It is calculated by summing all event-related spectrograms and dividing by the number of event trials. Since it is a running average, the spectrogram is recalculated and plotted with each new event.

(2) *Average plot on MR*. It displays running average event-related activations on the subject's 3D MRI surface reconstruction image.

(3) *Single-trial raster plot*: It displays single-trial activations in a stacked raster plot. Power from only one frequency band is shown.

(4) *Single plot*. It displays the event-related spectrogram of the most recent single event trial.

(5) *Continual plot*: It displays the mean z-score of the last 20 ms of data from a specified frequency.

All event windows were taken from 500 ms prior to the onset of the event, and 500 ms after the onset. The z-score measurements were presented using a normalized color scale.

To remove common artifact data, we implemented an algorithm for removing trials from occasionally corrupted noisy data caused by faulty electrodes in the average plot and single-trial raster. A window of data for a particular frequency band was deemed an artifact if more than 50% of the event window was below 1.5 baseline standard deviations or if more than 80% was above 1.5 baseline standard deviations. These data were displayed with a solid band of green on the plot itself.
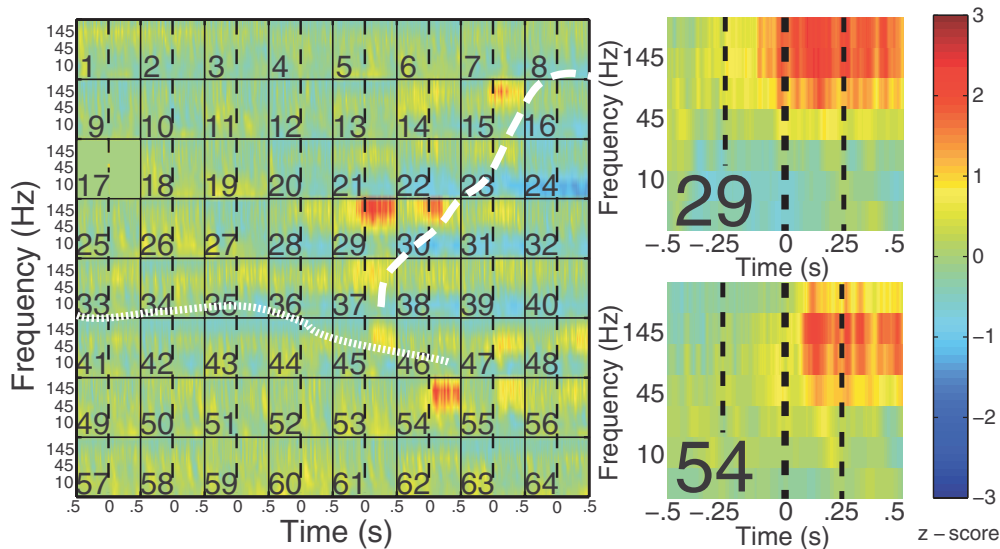
Figure 2. Average event-related spectrogram. Plots generated in real-time depict average event-related spectrograms for subject A (figure 1(A)). Each electrode is represented as a square on the 8 × 8 grid, and has its own separate time–frequency axes. The horizontal axis represents the progression of time, with the dotted line representing the onset of the event. Averaged data from half a second before the event to half a second after the event are displayed. The seven frequency bands are shown on the vertical axis (4–7, 8–12, 13–30, 31–59, 61–110, 111–179, 181–260 Hz). The central sulcus and Sylvian fissure are outlined with dashed and dotted lines, respectively. The average plot was generated after the subject produced the syllable /la/ for approximately 1 min. Spectrograms for specific channels are plotted on the right.

Electrical cortical stimulation

ECS mapping was performed on subjects with the 64-channel grid (subjects A–D) according to clinical motor mapping routines in 2–3 h sessions over 1–2 days. These procedures utilized constant current bipolar electrical stimulation between pairs of adjacent electrodes using a Grass S-88 cortical stimulator (Grass-Telefactor, West Warick, RI, USA). Trains of 1–5 s, 50 Hz, 0.3 ms, alternating polarity square-wave pulses were sent through the stimulator starting with an intensity of 1 mA. The intensity was increased at 1 mA increments, up to a maximum of 15 mA. Intensities were adjusted so that after-discharges were not produced. Patients reported any unusual or involuntary sensations or movements. Disruption of motor function was detected by observing patients during voluntary movements. It should be noted that not all electrode sites were stimulated. Sites suitable for stimulation were determined entirely by clinical neurologists and were dependent on the patient and probable resection and/or eloquent cortical areas.

Median nerve stimulation

Due to the high-density electrode configuration of subject E, standard ECS mapping was not carried out. However, standard localization of the central sulcus using the phase reversal of somatosensory evoked potential (N20–P20) was performed [27]. The contralateral median nerve was stimulated at the wrist with 5.1 pulses s^{-1} and a current intensity between 5 and 10 mA until twitches of the thumb were observed visually. The anode was placed just proximal to the palmar crease, and the cathode was placed between the tendons of the palmaris longus muscle, 3 cm proximal to the anode. ECoG signals were recorded simultaneously. The raw time series was averaged over 187 trials.

Results

Our system can be used to perform sensorimotor mapping using an event-triggered analysis in real-time within seconds (see the supplementary video available at stacks.iop.org/JNE/9/046018/mmedia).

Visualization

We first demonstrate that our method can be used to detect electrode-specific event-related spectral alterations. In the following presentation of data, neural activity is represented as z-score deviations from the baseline signal (depicted by a color scale). The event onset is denoted by a vertical dotted line at time 0 ms. Each plot portrays all channels from the entire subdural array. In this section, we discuss the three visual displays believed to be most pertinent to this study. The analysis of the single plot and continual plot is included in the supplementary material (figure s2) available at stacks.iop.org/JNE/9/046018/mmedia.

Average plot. The average plot shows the running average event-related spectrogram, which is updated in real-time after each event trial. The average plots from subjects A and E for the speaking and button press tasks are shown in figures 2 and 3. Additional plots are included in the supplementary material (figure s1) available at stacks.iop.org/JNE/9/046018/mmedia. It can be easily seen which electrodes are active immediately before and after the event onset. Thus, the average plot illustrates the localization of cortical functionality (e.g. sensory versus motor) based on the temporal patterns of activation while the patient is performing the task.
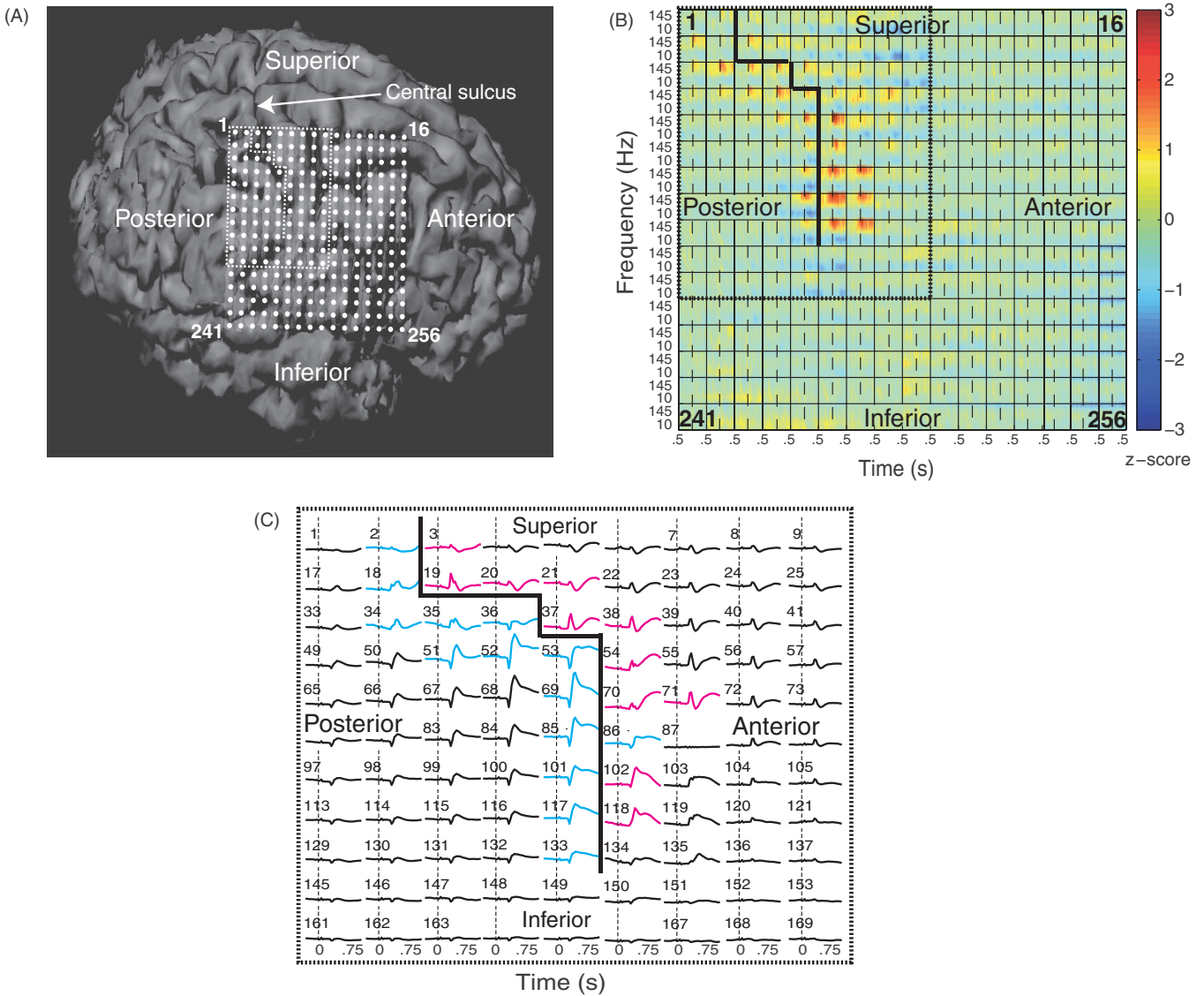
Figure 3. ECoG grid superimposed on patient brain, average event-related spectrogram and median nerve stimulation results. (A) A 256-channel subdural ECoG electrode array implanted over subject E's right lateral hemisphere. Electrodes are superimposed on the 3D MR surface reconstruction image. The boundary of the N20–P20 phase reversal is outlined. (B) Plots generated in real-time depict average event-related spectrograms during the button press task (task 3). Each electrode is represented as a square on the 16 × 16 grid, and has its own separate time–frequency axes. The horizontal axis represents the progression of time, with the dotted line representing the onset of the event. Averaged data from half a second before the event to half a second after the event are displayed. The seven frequency bands are shown on the vertical axis (4–7, 8–12, 13–30, 31–59, 61–110, 111–179, 181–260 Hz). The boundary of the N20–P20 phase reversal is outlined. (C) Somatosensory evoked potentials gathered during median nerve stimulation. Onset of stimulation is indicated with a dotted line at time 0 s. A phase reversal of the N20–P20 peak between a pair of electrodes indicates that the pair straddles the central sulcus. The blue potentials denote those that displayed a N20 peak during median nerve stimulation. The red potentials indicate that a P20 peak was seen during stimulation. The boundary of the N20–P20 phase reversal is outlined.

In figure 2, the average plot is shown for the evoked spectrograms when the subject repeated the syllable /la/ (task 1). Electrodes 15, 29 and 30 in the ventral precentral gyrus (primary motor cortex) show strong activation that is clearly event-locked, and begins slightly before event onset (−118 ms), suggesting the efferent neural motor commands for articulation. Electrode 29 demonstrated tongue movement with ECS. It can be seen that electrode 54 in the posterior superior temporal gyrus also reveals an increase in activity; however, this only occurs after event onset (72 ms), and

therefore is related to auditory afferent sensory processing (feedback of hearing oneself speak). Anomic speech arrest was found to occur at electrode 54 during ECS mapping while the patient was tested with confrontational picture naming. Key channels from the plot can be more carefully examined on the right. Previously, the delineation of motor from sensory sites was done in offline analyses [12, 16, 17].

In figure 3, the utility of real-time spectral mapping of sensory and motor organization for the hand is shown. Subject E was implanted with a 256-channel array over the right
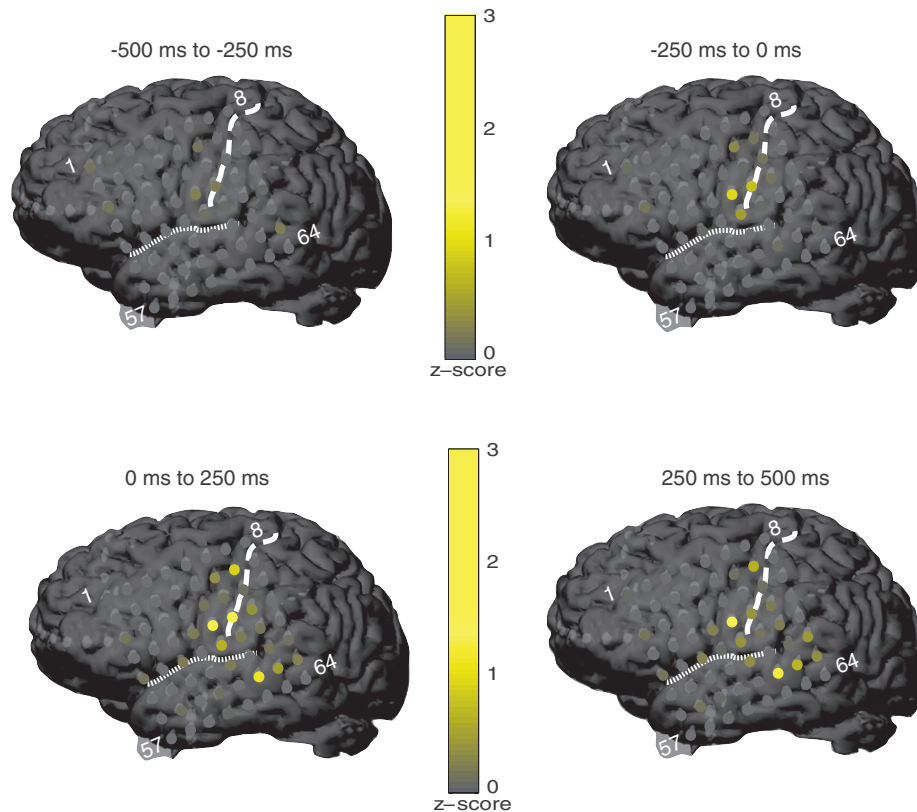
Figure 4. Average activity at different time epochs on MRI surface reconstruction. Plots generated in real-time depict average event-related high gamma (61–260 Hz) activations on subject A's 3D MRI surface reconstruction image at four different time intervals (−500 to −250 ms, −250 to 0 ms, 0 to 250 ms, 250 to 500 ms) during production of the syllable /la/. The central sulcus and Sylvian fissure are outlined with dashed and dotted lines, respectively.

peri-Rolandic cortex (figure 3(A)). The average plot was generated in real-time while subject E was pressing a button with his left thumb (figure 3(B), see the supplementary video available at stacks.iop.org/JNE/9/046018/mmedia). Electrodes along the central sulcus can be rapidly visually identified to have an event-related increase in the high gamma power (61–260 Hz), and an event-related decrease in alpha power (4–12 Hz), consistent with previous findings [12, 13]. The anterior ventral-most electrodes showed high gamma activation onset nearly 200 ms prior to the button press, consistent with the precentral gyrus cortical motor processing specifically for the thumb which is the most ventral representation in the homunculus. In contrast, the posterior electrodes showed somatosensory activation after the button press. Using median nerve stimulation, the typical N20–P20 phase reversal in the averaged evoked potentials is observed along the central sulcus (figure 3(C)), and confirmed the localization mapping from real-time spectral mapping. Note that median nerve stimulation is not exactly identical to thumb movement alone in the button press, which may explain some of the minor differences in localization between the plots.

Spatial layout of electrodes over the MRI surface reconstruction at different time epochs. In order to provide an intuitive visualization which readily relates activity to anatomical regions, the magnitude of the running average

event-related high gamma (61–260 Hz) activations at four different time intervals (−500 to −250, −250 to 0, 0 to 250, 250 to 500 ms) was projected on to the subject's 3D MRI surface reconstruction image, and updated after every trial. Plots from the same speech production task (/la/) are shown in figure 4. It can be easily seen which electrodes are active immediately before and after the event onset, and where they are located on the subject's individual brain. The four separate time epochs allow one to distinguish the pre-event motor from post-event sensory cortical activations.

Single-trial raster plot. The raster plot displays cumulative single-trial spectral changes for a given frequency range (111–179 Hz used for this example) measured in z-score deviations from the baseline. The stacked single-trial plot was generated simultaneously with the same speech production task (/la/), and is shown in figure 5. For each new event, the plot was updated in real time with the single event trial added as a horizontal row.

The patterns observed across events demonstrate the robustness of the physiologic approach in single trials, and provide a visualization that is not susceptible to outlier values (in contrast to the average plots). Key channels from the raster plot can be more carefully examined on the right. Note that the time axis has been extended to show a full second after the event. Again, these plots demonstrate that activity
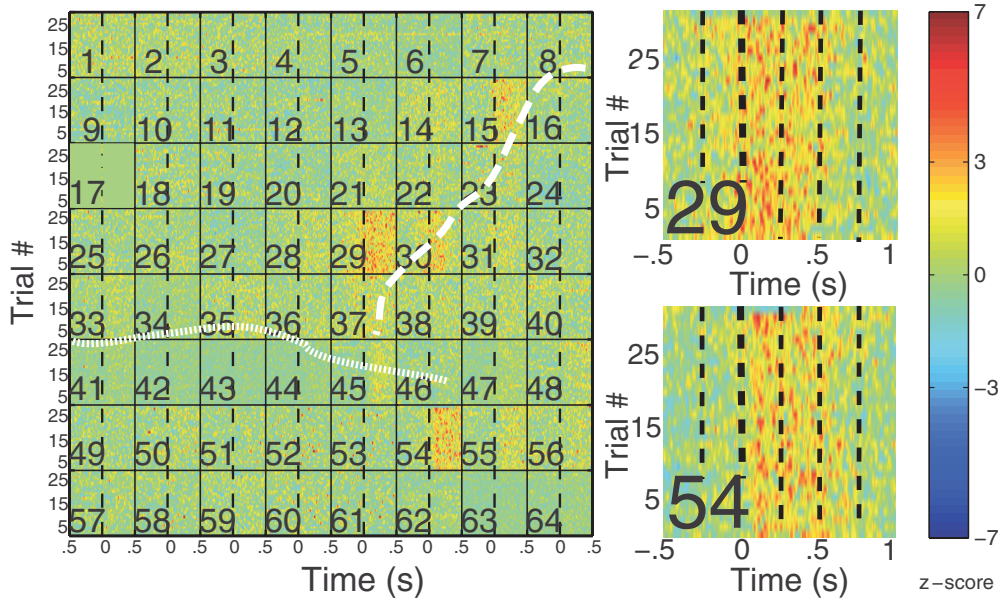
Figure 5. Single-trial raster plots. Plots generated in real-time depict single-trial raster plots for subject A's 8 × 8 electrode grid (figure 1(A)). Each electrode has its own separate time axes. The horizontal axis represents the progression of time, with the dotted line representing the onset of the event. Data from half a second before the event to half a second after the event are displayed. On the vertical axis are each event's activations in one frequency band (111–179 Hz). Z-score deviations from the baseline are in colorscale. This raster plot was generated after the subject produced the syllable /la/ for approximately 1 min. The central sulcus and Sylvian fissure are outlined with dashed and dotted lines, respectively. Rasters for specific channels are plotted on the right. The time axis has been extended to show a full second after the event.
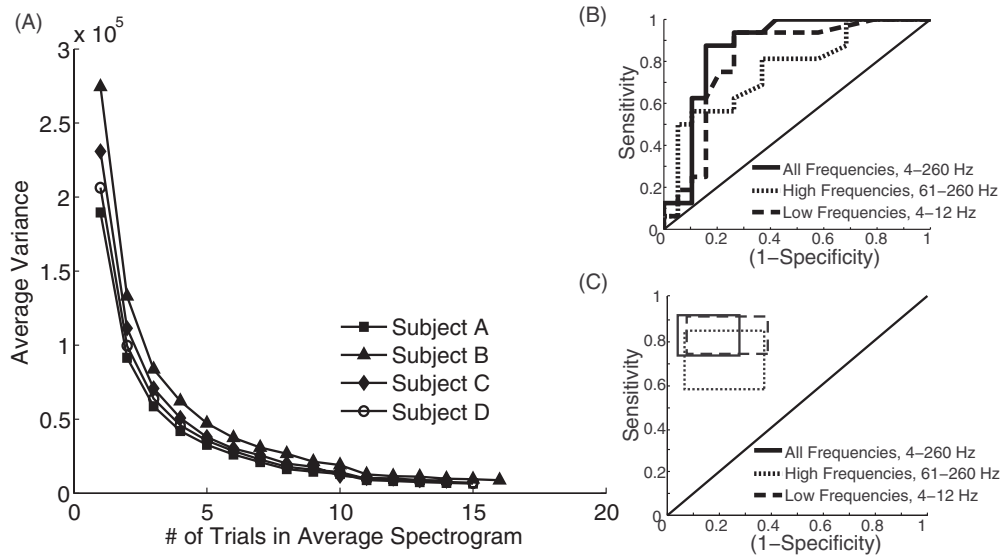

Figure 6. Average variance and sensitivities and specificities for subjects. (A) The average variance of average plots is shown as a function of the number of trials incorporated into the average. (B) Subject C's ROC curve. Electrode channels were categorized as positive or negative using average squared-z-scores and compared against ECS maps. Z-scores from the average spectrogram after the tenth trial were used. Three spectral ranges were examined (4–260, 61–260, 4–12 Hz). The ROC curve plots the rate of true positives (sensitivity) against the false positive rate (1-specificity). The diagonal line (line of no-discrimination) divides the ROC space between good and poor classification results. Values in the upmost left corner indicate perfect classification. (C) Using all four subjects, sensitivities and specificities ranges (95% confidence intervals) were found using subject-specific optimal thresholds and plotted in the ROC space.

occurs earlier in the motor electrodes compared to the sensory auditory channels.

Robustness of the running average visualization. To examine the robustness of our algorithm, the variance of running average spectrograms was analyzed offline for subjects with ECS mapping results. All N trials within an experiment were randomized and binned to contain n number of trials in each bin (n ranging from 2 through N/2). An average spectrogram was then created from each bin of trials and a mean and variance between these spectrograms were calculated. It is important to note that no one trial is used in

more than one average spectrogram; thus, no bias is created. This was repeated 100 times and the average variance was calculated as a function of number of trials (figure 6(A)). A sharp exponential decay exists across all subjects. The variance between average spectrograms becomes minimal after incorporating approximately five trials in the average, and virtually negligible after ten events. This suggests that a very stable representation of cortical activity is achieved with very few repetitions.

Sensitivity and specificity. The sensitivity and specificity of our mapping algorithm were analyzed offline for subjects A–D at overlapping ECS sites. Sites below the Sylvian fissure were discarded since our tasks and ECS results targeted primarily the motor and somatosensory cortex that are usually mapped with ECS. Three sets of data were used: the average spectrogram z-scores after the first ten trials for (i) all frequencies (4–260 Hz), (ii) the low frequencies (4–12 Hz) and (iii) the high frequencies (61–260 Hz). Sites were deemed positive (+) if the average-squared z-score exceeded some threshold ranging from 0 to 2 with 0.01 increments, and deemed negative (−) otherwise. ECS sites were categorized by neurologists as (+) if stimulation produced unusual or involuntary sensations or movements during clinical motor mapping, and (−) otherwise. Although adjacent electrodes were stimulated together, each site was counted separately so that the two mapping techniques could be compared.

A receiver operating characteristic (ROC) curve and the area-under-the-ROC-curve (AUC) were calculated using ECS results as the correct classification. Subject-specific ROCs are shown in figure 6(B) and in the supplementary material (figure s3) available at stacks.iop.org/JNE/9/046018/mmedia. Averaging across patients, AUC confidence intervals were found for the three sets of data. Using all frequencies, the AUC was 0.85 ± 0.083 (95% confidence interval). High-frequency data yielded an AUC range of 0.73 ± 0.11 (95% confidence interval). Using low frequencies, the AUC range was 0.79 ± 0.10 (95% confidence interval). To verify that analyses were not biased from using only one baseline per day of experimentation, data were reanalyzed offline by renormalizing the data from each experimental session with its own baseline. These results were not significantly different, and suggest that only one baseline collection is necessary per day of experimentation.

The optimal threshold—defined as the threshold that yielded the sensitivity and specificity coordinate pair closest to 100% classification accuracy on the ROC curve—varied across subjects. With high-frequency data, and using the subject-specific optimal threshold, the sensitivity was $70.8 \pm 13.4\%$ (95% confidence interval) relative to ECS (+) sites. The specificity was $78.1 \pm 15.3\%$ (95% confidence interval) relative to ECS (−) sites. For the low frequencies, the sensitivity was $82.1 \pm 8.5\%$ (95% confidence interval) and the specificity was $77.0 \pm 15.6\%$ (95% confidence interval). Using all frequencies, the sensitivity was $82.0 \pm 9.2\%$ (95% confidence interval) and the specificity was $84.2 \pm 11.9\%$ (95% confidence interval). These intervals are depicted in figure 6(C). Again, data using baselines from the same experimental session were not significantly different.

Discussion

This paper describes a novel technique for real-time signal analysis that can safely localize physiologic cortical function within seconds. Novel instantaneous visualization of average and single-trial activity with clear spatial and temporal resolution allow for quick visual assessment of cortical function.

Of late, there have been several impressive demonstrations of real-time brain mapping [19–23]. In particular, Schalk *et al* sought to identify sensorimotor cortex using a modified competitive expectation maximization statistical method called SIGFRIED. Their powerful method was able to provide a visual interface for the localization of isolated electrodes covering pertinent cortical regions. Our results extend these pioneering efforts to provide critical temporal resolution that is needed to differentiate temporal phases of activity, including those between sensory and motor cortex— an essential attribute to any clinically performed functional mapping. As figures 2–5 demonstrate, our visualizations are capable of highlighting temporal and spectral differences between electrodes that can give clinical investigators insight into such functional differences without the need of *a priori* thresholds.

Comparing our algorithm's results to those obtained by ECS, we conclude that we can reasonably classify positive and negative electrodes in the low- and high-frequency domains, and can classify remarkably well when all frequencies are used. In addition, we see an exponential decay in variance between running average spectrograms. This suggests that very few repetitions (five to ten event trials) are needed to obtain a stable functional map. Indeed, the single-trial raster plots demonstrate that much of the evoked neural activity can be observed on a per trial basis. This helps to interpret potential confounds in the average plots generated from outlier data. With a more extensive battery of tests, we believe that this method is capable of mapping critical eloquent cortex (e.g. expressive languages, sensory, motor) within minutes, with minimal effort required from the patient and no morbidity.

A few plausible explanations exist to explain the discrepancies between our algorithm's and ECS maps. First, it is difficult to compare methodologies due to the inherent differences in approaches. For example, due to the all-or-none nature of ECS responses, it is necessary for our comparison to also analyze ECoG data using a simple positive-or-negative threshold [7]. However, inter-subject variation in the ECoG signal and behavior makes it difficult to define an absolute threshold. In addition, clinical stimulation procedures require pairs of electrodes to be stimulated together. Bipolar stimulation is thought to be more spatially specific as the current is localized between the two electrodes, whereas unipolar stimulation is thought to be less specific as the current can spread unpredictably to the corticospinal tract. In this study, we count electrodes of a (+) stimulation pair as two separate (+) sites, which may over-count the number of true positive sites. Furthermore, ECS evokes non-physiologic stereotyped movements. This is fundamentally different from our method, which is designed to capture cortical activity that occurs during normal behavioral movement.

Another explanation may be that ECS itself can be erroneous. ECS-induced after-discharges often spread to cortex outside the current field, thereby overestimating the extent of functional cortex [5, 6, 9, 28, 29]. Thresholds for ECS mapping can be extremely variable between individuals, and in some cases, no motor sites can be detected despite exhaustive testing. Thus, it is possible that ECS is less specific than previously assumed, and perhaps does not replace the ultimate gold-standard, which is patient neurological outcome.

Limitations in our own methods may also account for discrepancies. One such limitation is that our method relies on collecting a baseline rest period, and re-referencing to the common average. Outliers (e.g. seizure activity, movements, poor signal-to-noise ratio) could affect results by skewing baseline statistics or the common average used to calculate relative change during event-related activity. For example, contamination of the baseline could lead to a more variable signal, making it more difficult to detect significant event-related spectral alterations using a z-score, which is sensitive to the variance of the baseline. Thus, the contaminated signal could potentially lead to a higher number of false negatives and lower sensitivity rates. Since using different baselines did not significantly change our results, it seems unlikely that our results were adversely affected by noisy baselines. However, this limitation highlights the importance of monitoring for outlier activity during experimentation. We currently visually reject electrodes with poor signal quality. Although susceptible to human error, this is common practice among clinicians and researchers. Future studies can evaluate the automation of this process using the known biophysical properties of ECoG recordings to reject artifact-laden signals [30]. In addition, we plan to explore methods of isolating motor elements from cortical maps that do not require baseline statistics, such as subtraction of sensory activations.

Additionally, the current study performed only four tasks that were designed to highlight sensorimotor cortical regions during speech production and hand movement. However, motor stimulation mapping routines are tailored to specific individuals, which lead to a variable number of stimulation sites and differing responses between patients. For example, subject A had a limited number of sites tested during stimulation, which could account for the high sensitivity and specificity rates (figure s3(A) available at stacks.iop.org/JNE/9/046018/mmedia). Stimulation for some patients also elicited wrist movement, and throat movement. Our tasks did not require strong wrist or throat movements, and thus our algorithm could not have been expected to detect these (+) sites.

The determination of a diagnostic 'threshold' does have significant implications for the long-term clinical application of our approach. While it offers a novel method for the determination of local cortical processing, our algorithm needs validation across many patients across institutions to carefully assess a threshold that maintains high sensitivity and specificity.

For these reasons, we have strongly advocated direct representation of the data analysis (e.g. illustrating complete spectrograms for each electrode, both single trial and average, in addition to the high gamma plots alone) since a simple threshold-derived 'yes/no' response may be misleading. For now, this method will require users to have some familiarity with signal processing involved to make safe decisions about its clinical application.

The ethical considerations for adoption of this mapping tool are similar to those of other tools used for preoperative or pre-resection mapping, such as functional magnetic resonance imaging or magnetic source imaging. That is, there needs to be clear benefit to the patient from this new technology. To achieve this, future studies must prospectively validate that it is more effective or equivalent than the current standard of ECS mapping. Our paper is the first step in describing the technology. At this point, we use these findings only to supplement stimulation mapping.

The speed, accuracy and safety of this algorithm make it a promising candidate for future applications in both clinical and basic research, but there are several ways in which our mapping method can be further developed. To improve upon the clinical utility of this system, subsequent developments will examine different user interfaces that might be useful to clinicians, such as anatomically derived coordinate systems and easy-to-use graphical user interfaces.

Acknowledgments

References

[1] Penfield O and Jasper M 1954 Epilepsy and the functional anatomy of the human brain *JAMA* **155** 86
[2] Penfield W and Roberts L 1959 *Speech and brain mechanisms* (Princeton, NJ: Princeton University Press)
[3] Haglund M, Berger M, Shamseldin M, Lettich E and Ojemann G 1994 Cortical localization of temporal lobe language sites in patients with gliomas *Neurosurgery* **34** 567
[4] Keles G, Lundin D, Lamborn K, Chang E, Ojemann G and Berger M 2004 Intraoperative subcortical stimulation mapping for hemispheric perirolandic gliomas located within or adjacent to the descending motor pathways: evaluation of morbidity and assessment of functional outcome in 294 patients *J. Neurosurg.* **100** 369–75
[5] Luders H, Lesser R, Hahn J, Dinner D, Morris H, Wyllie E and Godoy J 1991 Basal temporal language area *Brain J. Neurol.* **114** 743
[6] Nii Y, Uematsu S, Lesser R and Gordon B 1996 Does the central sulcus divide motor and sensory functions *Brain* **46** 360–7
[7] Sinai A, Bowers C, Crainiceanu C, Boatman D, Gordon B, Lesser R, Lenz F and Crone N 2005 Electrocorticographic high gamma activity versus electrical cortical stimulation mapping of naming *Brain* **128** 1556–70
[8] Ojemann G, Ojemann J, Lettich E and Berger M 1989 Cortical language localization in left, dominant hemisphere: an electrical stimulation mapping investigation in 117 patients *J. Neurosurg.* **71** 316–26
[9] Lesser R, Luders H, Klem G, Dinner D, Morris H and Hahn J 1984 Cortical afterdischarge and functional response thresholds: results of extraoperative testing *Epilepsia* **25** 615–21

[10] Krauss G L, Fisher R, Plate C, Hart J, Uematsu S, Gordon B and Lesser R P 1996 Cognitive effects of resecting basal temporal language areas *Epilepsia* **37** 476–83

[11] Ojemann G 1979 Individual variability in cortical localization of language *J. Neurosurg.* **50** 164–9

[12] Crone N, Miglioretti D, Gordon B and Lesser R 1998 Functional mapping of human sensorimotor cortex with electrocorticographic spectral analysis: II. Event-related synchronization in the gamma band *Brain* **121** 2301

[13] Crone N, Miglioretti D, Gordon B, Sieracki J, Wilson M, Uematsu S and Lesser R 1998 Functional mapping of human sensorimotor cortex with electrocorticographic spectral analysis: I. Alpha and beta event-related desynchronization *Brain* **121** 2271

[14] Pfurtscheller G, Graimann B, Huggins J, Levine S and Schuh L 2003 Spatiotemporal patterns of beta desynchronization and gamma synchronization in corticographic data during self-paced movement *Clin. Neurophysiol.* **114** 1226

[15] Canolty R T, Soltani M, Dalal S S, Edwards E, Dronkers N F, Nagarajan S S, Kirsch H E, Barbaro N M and Knight R T 2007 Spatiotemporal dynamics of word processing in the human brain *Front. Neurosci.* **1** 185

[16] Chang E F, Edwards E, Nagarajan S S, Fogelson N, Dalal S S, Canolty R T, Kirsch H E, Barbaro N M and Knight R T 2010 Cortical spatio-temporal dynamics underlying phonological target detection in humans *J. Cogn. Neurosci.* **23** 1437–46

[17] Edwards E, Nagarajan S S, Dalal S S, Canolty R T, Kirsch H E, Barbaro N M and Knight R T 2010 Spatiotemporal imaging of cortical activation during verb generation and picture naming *Neuroimage* **50** 291–301

[18] Crone N, Hao L, Hart J Jr, Boatman D, Lesser R, Irizarry R and Gordon B 2001 Electrocorticographic gamma activity during word production in spoken and sign language *Neurology* **57** 2045

[19] Lachaux J, Jerbi K, Bertrand O, Minotti L, Hoffmann D, Schoendorff B and Kahane P 2007 A blueprint for real-time functional mapping via human intracranial recordings *PLoS One* **2** 1094

[20] Miller K, denNijs M, Shenoy P, Miller J, Rao R and Ojemann J 2007 Real-time functional brain mapping using electrocorticography *Neuroimage* **37** 504–7

[21] Schalk G, Leuthardt E, Brunner P, Ojemann J, Gerhardt L and Wolpaw J 2008 Real-time detection of event-related brain activity *Neuroimage* **43** 245–9

[22] Brunner P *et al* 2009 A practical procedure for real-time functional mapping of eloquent cortex using electrocorticographic signals in humans *Epilepsy Behav.* **15** 278–86

[23] Roland J, Brunner P, Johnston J, Schalk G and Leuthardt E C 2010 Passive real-time identification of speech and motor cortex during an awake craniotomy *Epilepsy Behav.* **18** 123–8

[24] Duffau H 2012 The 'frontal syndrome' revisited: lessons from electrostimulation mapping studies *Cortex* **48** 120–31

[25] Fox P T and Friston K J 2012 Distributed processing; distributed functions? *Neuroimage* **61** 407–26

[26] Siegel M, Donner T H and Engel A K 2012 Spectral fingerprints of large-scale neuronal interactions *Nature Rev. Neurosci.* **13** 121–34

[27] Dinner D S, Luders H, Lesser R P and Morris H H 1987 Cortical generators of somatosensory evoked potentials to median nerve stimulation *Neurology* **37** 1141

[28] Blume W, Jones D and Pathak P 2004 Properties of after-discharges from cortical electrical stimulation in focal epilepsies *Clin. Neurophysiol.* **115** 982–9

[29] Motamedi G, Lesser R, Miglioretti D, Mizuno Matsumoto Y, Gordon B, Webber W, Jackson D, Sepkuty J and Crone N 2002 Optimizing parameters for terminating cortical afterdischarges with pulse stimulation *Epilepsia* **43** 836–46

[30] Miller K J, Sorensen L B, Ojemann J G and den Nijs M 2009 Power-law scaling in the brain surface electric potential *PLoS Comput. Biol.* **5** e1000609